Nano Energy 104 (2022) 107992

Contents lists available at ScienceDirect

Nano Energy

journal homepage: www.elsevier.com/locate/nanoen

A droplet-based triboelectric-piezoelectric hybridized nanogenerator for scavenging mechanical energy

Maoyi Zhang [a,b,d], Chengmin Bao [b,e], Chaosheng Hu [b,e], YongAn Huang [c], Ya Yang [b,e,*], Yewang Su [a,d,**]

[a] State Key Laboratory of Nonlinear Mechanics, Institute of Mechanics, Chinese Academy of Sciences, Beijing 100190, China
[b] CAS Center for Excellence in Nanoscience, Beijing Key Laboratory of Micro-Nano Energy and Sensor, Beijing Institute of Nanoenergy and Nanosystems, Chinese Academy of Sciences, Beijing 101400, China
[c] State Key Laboratory of Digital Manufacturing Equipment and Technology, Huazhong University of Science and Technology, Wuhan 430074, China
[d] School of Engineering Science, University of Chinese Academy of Sciences, Beijing 100049, China
[e] School of Nanoscience and Technology, University of Chinese Academy of Sciences, Beijing 100049, China

ARTICLE INFO

Keywords:
Water droplet
Triboelectric nanogenerator
Cantilever beam
Response time
Hybridized nanogenerator

ABSTRACT

Water droplet energy has received much attention as a newborn renewable energy source. Triboelectric nanogenerators (TENGs) demonstrates enormous application in scavenging mechanical energy. Nowadays, the water droplet nanogenerator based on liquid-solid TENG has been greatly improved. However, these water droplet nanogenerators scavenge the mechanical energy of liquid-solid contact of water droplets by TENG, but not the deformation energy of the substrate. Here, we propose a new design strategy to increase the current of the water droplet nanogenerator through simultaneous scavenging of the mechanical energy of the liquid-solid contact and the deformation energy. A droplet-based triboelectric-piezoelectric hybridized nanogenerator (TPiHNG) with cantilever beam structure was fabricated under the strategy. The TPiHNG has a significantly higher current compared to TENG. The response time difference between piezoelectric nanogenerator (PiENG) and TENG is proposed for the first time as an important parameter of TPiHNG. This work provides a novel approach to scavenge water droplet energy more efficiently.

1. Introduction

The need for energy is growing in tandem with the fast expansion of human society. Because of the rising depletion of fossil energy, the development and usage of renewable energy is increasingly critical [1–3]. Some renewable energy such as solar energy [4–7], geothermal energy [8–10], hydropower [11,12] and wind energy [13–18] have been widely utilized. The hydropower, one of the most abundant renewable energies, plays an indispensable role in the energy supply. Hydroelectric power stations built on rivers convert the potential energy of water into electrical energy through electromagnetic generators, which is an important application of hydropower [19,20]. In addition to the rivers containing huge amounts of water, there are also numerous tiny water droplets in hydropower. If water droplets can be utilized to their full potential, it is a powerful complement to renewable energy.

Triboelectric nanogenerators (TENGs) based on frictional initiation and electrostatic induction were first proposed in 2012 [21]. TENG demonstrates enormous application in the field of micro and nano energy due to easy fabrication and wide range of material choices [22,23]. TENG can be employed to scavenge mechanical energy not only in solid-solid contact [24–26] but also in liquid-solid contact [27–38]. After several years of development, the performance of liquid-solid TENG in scavenging water droplet energy has been greatly improved. Water droplet nanogenerators based on liquid-solid TENG emerged for the first time in 2014, opening a new path for efficient scavenging of water droplet energy [27]. The electrodes of these conventional water droplet nanogenerators are all located below the dielectric layer [29–31]. In 2020, a novel water droplet nanogenerator design inspired by transistors was proposed [28]. These novel water droplet nanogenerators have top electrodes on top of the dielectric layer [32–34]. By

* Corresponding author at: CAS Center for Excellence in Nanoscience, Beijing Key Laboratory of Micro-Nano Energy and Sensor, Beijing Institute of Nanoenergy and Nanosystems, Chinese Academy of Sciences, Beijing 101400, China.
** Corresponding author at: State Key Laboratory of Nonlinear Mechanics, Institute of Mechanics, Chinese Academy of Sciences, Beijing 100190, China.
E-mail addresses: yayang@binn.cas.cn (Y. Yang), yewangsu@imech.ac.cn (Y. Su).

https://doi.org/10.1016/j.nanoen.2022.107992
Received 9 September 2022; Received in revised form 24 October 2022; Accepted 5 November 2022
Available online 7 November 2022

converting the previous interfacial effect into the ideal bulk effect, the signal of the novel water droplet nanogenerator is greatly enhanced compared to the conventional one. Water droplets are available for a sustainable green energy source [39].

However, these water droplet nanogenerators have not fully scavenged the water droplet mechanical energy. They scavenged the mechanical energy of liquid-solid contact of water droplets by TENG, but not the deformation energy of the substrate. Piezoelectric nanogenerators (PiENGs) based on the piezoelectric effect can convert mechanical energy into electrical energy through the deformation of piezoelectric materials [40]. Currently PiENG has been widely used for deformation energy scavenging[41–44]. Inspired by the leaf-rain interaction, Xu et al. [45] develop a leaf-mimic rain energy harvester (REH) of cantilever beam structure utilizing TENG and PiENG to improve the transferred charge value by simultaneously scavenging energy from liquid-solid contact and beam vibration. TENG and PiENG in the REH have their own electrodes and charge the capacitors by gathering the charges together through separate connection to rectifier bridge.

Here, we propose a new design strategy to increase the current of the water droplet nanogenerator through simultaneous scavenging of the

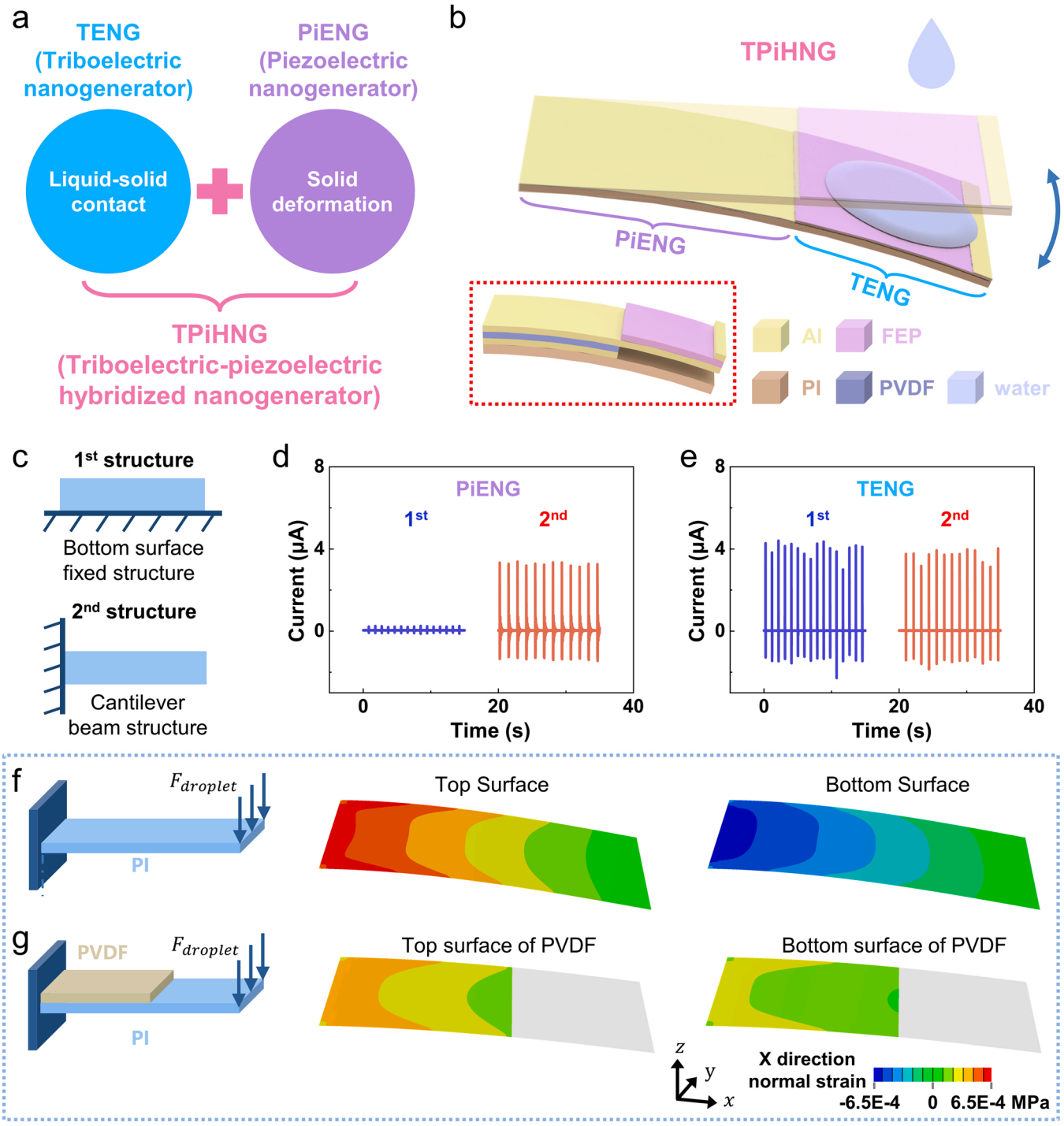

Fig. 1. Design and model of TPiHNG. (**a**) Design strategy of TPiHNG. (**b**) Model diagram of TPiHNG. (**c**) Two design structures. Comparison of currents of (**d**) PiENG and (**e**) TENG under two structures. Strain distribution along x-direction for (**f**) PI of cantilever beam structure and (**g**) PI of cantilever beam structure with PVDF attached.

mechanical energy of the liquid-solid contact of the water droplets and the deformation energy of the substrate, as shown in Fig. 1a. The droplet-based triboelectric-piezoelectric hybridized nanogenerator (TPiHNG) was fabricated under the strategy. Through experimental comparison, the cantilever beam structure was adopted as the structure of TPiHNG due to the better performance. The mounting direction of the piezoelectric material was determined through utilizing finite element analysis (FEA) simulation. The TPiHNG has a significantly higher current compared to TENG. The response time difference between PiENG and TENG is proposed for the first time as an important parameter of TPiHNG. The effects of different variables on the currents of TENG, PiENG, TPiHNG and the response time difference between PiENG and TENG were investigated. This work provides a novel approach to scavenge water droplet energy more efficiently.

2. Experimental section

2.1. Fabrication of TPiHNG

At first, a 40 mm × 30 mm × 50 μm double-sided aluminized polyvinylidene fluoride (PVDF) film (Jinzhou Kexin Dianzi Cailiao Co., LTD, China) is attached to a 70 mm × 30 mm × 225 μm Polyimide (PI) film with double-sided adhesive. Then, the rest of the PI film surface is covered with aluminum (Al) tape and the Al tape is in contact with the Al electrode on top of the PVDF film. After that, the fluorinated ethylene propylene (FEP) film with glue is taped onto the Al tape. Finally, a small strip of Al tape is placed on the FEP film.

2.2. Experiments and electrical measurements

Ultrapure water (resistivity is 18.2 MΩ·cm) and pure water (conductivity is 10.9 μs/cm) come from laboratory water purification systems (HHitech Co., China). Generally, slope angle, falling height, falling frequency, water source and volume in the experiment were 10-degree, 85 cm, 1 Hz, ultrapure water and 60 μl. The water droplet impact position is not easy to control. In general, the impact position is around position 3. The impact position is guaranteed to remain constant during each group of the measurements. An electrometer (Keithley 6514) with sampling frequency of 5000 Hz was chosen to measure the current. The nanogenerator and Keithley 6514 were connected directly in series without connecting external resistance to measure current. The voltage measurement was made by connecting the nanogenerator and Keithley 6514 directly in parallel without connecting external resistance.

2.3. FEA simulation

ABAQUS was adopted as the software for the FEA simulation. PI and PVDF were treated as the linear elastic materials. Poisson's ratio of the PI was 0.34 and the elastic modulus was 2.5 GPa. The geometry of the PI film was 70 mm × 30 mm × 225 μm, as shown in Fig. 1f. PVDF had an elastic modulus of 2.5 GPa and a Poisson's ratio of 0.35. As shown in Fig. 1g, the geometry of PVDF film was 40 mm × 30 mm × 50 μm. PI film and PVDF film adopted the shell element S4R.

3. Results and discussion

The performance of PiENG with different structures is different. In order to acquire TPiHNG with better performance, the structure of PiENG was investigated. Two common structures of PiENG can be selected, as shown in Fig. 1c. The first structure is the bottom surface fixed structure, which is commonly employed for the substrate of liquid-solid TENG [28,32–34]. The second structure is the cantilever beam structure. The cantilever beam structure has a greater strain than the bottom surface fixed structure, so the PiENG with the cantilever beam structure can obtain larger voltage [46]. Therefore, previous researchers usually consider the PiENG as the cantilever beam structure [47–49]. However, the current of PiENG is positively related to the strain rate, which is not related to the strain [50]. In order to compare the piezoelectric current magnitude of the two structures, experimental measurements were conducted. The piezoelectric current of the cantilever beam structure is 3.3 μA, which is substantially greater than the 0.2 μA of the bottom fixed structure, as shown in Fig. 1d. We also compared the currents of the two structures of the TENG and found that the current of the cantilever beam structure was slightly smaller than that of the bottom fixed structure, as shown in Fig. 1e. Therefore, we designed the TPiHNG as cantilever beam structure.

PVDF was chosen as the piezoelectric material for the TPiHNG. Since the thickness of PVDF film is much smaller than the width and length, the effect of piezoelectric strain constant d_{33} on the current is neglected. d_{31} of PVDF is much larger than d_{32}, so the 11 direction of PVDF is kept parallel to the x direction of the cantilever beam when placing PVDF film (Fig. 1g). The current direction of the piezoelectric material is opposite when it is under tension and compression. In order to make the current directions of PiENG and TENG the same, we investigated the strain distribution along the x-direction of the cantilever beam structure by FEA simulation. The impact load of water droplets on the cantilever beam was simplified to the normal load acting on the free end of the cantilever beam with the linear distribution. Under the normal load, the cantilever beam bends downward and the top surface of the cantilever beam is subjected to tension and the bottom surface to compression, as shown in Fig. 1f. When placing the PVDF film on the top surface of the end of the cantilever beam, both the top and bottom surfaces of the PVDF film are subjected to tension due to the thin thickness of the PVDF film (Fig. 1g). For the case of PVDF film under tension, we place the PVDF film with the polarization direction facing downward to ensure that the current direction of PiENG and TENG is the same.

Theoretically when the cantilever beam bends, the displacement of the free end of the cantilever beam is greater than that of the cantilever anchor, and the strain of the cantilever anchor is greater than that of the free end of the cantilever beam (Fig. 1f). Therefore, the piezoelectric current generated by the cantilever anchor's PVDF film is larger than that of the free end of the cantilever beam. So, we placed the PVDF film at the end of the cantilever anchor in the device design. To confirm the theory, we compared the piezoelectric currents of the device with PVDF film located at the free end of the cantilever beam and the device with PVDF film located at the cantilever anchor. Fig. S1a and Fig. S1b show that the current at the free end of the cantilever beam (3.65 μA) is slightly larger than that of the cantilever anchor (3.16 μA). In order to find the reason why the experimental results were not expected, the current waveform of the free end of the cantilever beam was carefully analyzed. When the water droplet leaves the cantilever beam, the cantilever beam does damped free vibration. As shown in Fig. S1c and Fig. S1d, the attenuation current (in the purple box) of the cantilever beam anchor is evident, while the attenuation current (in the purple box) of the free end of the cantilever beam is almost missing. This confirms that the theory is correct. When the cantilever beam bends, the strain of the cantilever anchor is larger than that of the end of the cantilever beam (Fig. 1f). As shown in Fig. S1f, the initial current at the end of the cantilever beam is negative, which is very strange. The PVDF film located at the end of the cantilever beam is compressed in the thickness direction (z-direction) when the PVDF film is impacted by water droplets. A compression in the thickness direction means a pull in the length direction (x-direction) and width direction (y-direction). The initial current should be positive. The PVDF film located at the cantilever anchor is pulled in the length direction when the water droplet impacts. Theoretically the initial current is positive, which is consistent with the experimental results (Fig. S1e). We infer that the initial current is negative because when the PVDF film is glued to the PI with double-sided tape, the PVDF film wrinkled. When the water droplets impacted on the wrinkled place will cause the PVDF film compression in the length direction. So, the initial current is negative. When the impact force disappears, the area under pressure recovers, so the current is

positive. As the wrinkled area is not large, so the two current peaks are relatively sharp. Utilizing wrinkling is an approach to increase the maximum current, which can be focused on in the future. Since the theory of cantilever beam bending is clearer and the current of wrinkling is only a little higher than that of bending, here we still employ the method of cantilever beam bending to design the device.

Based on the foregoing, we designed the TPiHNG with cantilever beam structure which is shown in Fig. 1b. The physical diagram of TPiHNG is shown in Fig. S2. The PiENG is located on the cantilever beam's side close to the fixed end, while the TENG is located on the side close to the free end. They share one electrode. The circuit diagram of the TPiHNG is shown in Fig. S3. The PiENG and TENG are connected in parallel. The bottom electrode of the PiENG and the top electrode of the TENG are one output of the TPiHNG. The common electrode of the PiENG and TENG is another output of the TPiHNG. There are six layers in the TPiHNG. Count from the bottom to the top, starting with the supporting layer at the bottom, which is formed of PI. Al film, which serves as PVDF's bottom electrode, is the second layer. The third layer is PVDF film. PVDF and its bottom electrode only cover the part of PI near the fixed end. The fourth layer is the Al film which covers the whole PI, The Al film is both the top electrode of PVDF and the bottom electrode of TENG, which is a common electrode. The fifth layer is the FEP film as the friction layer of TENG, which only covers the part of PI near the free end. The sixth layer is the Al film as the top electrode of TENG.

The currents of TENG, PiENG and TPiHNG were investigated through experiments. As shown in Fig. 2a and b, the currents of TENG and PiENG are 3.7 μA and 3.3 μA, respectively. The current of TPiHNG is 6.2 μA (Fig. 2c), which is 1.7 times of the current of TENG, indicating that the hybrid design effectively increases the current. The current of TENG is smaller than other literatures [28,33,34], which we think is caused by the different friction layer material, friction layer thickness and water source [34,51]. The current of TENG in Xu et al.'s work [45] is high due to the suitable friction layer material and thickness. It is not meaningful to increase the current by parallel connection, so Xu et al. improve the performance by increasing the charge. When limited by the friction layer material and material thickness, the output current of TENG is small and can be increased by parallel connection. There is significant difference between the current waveforms of TENG and PiENG. The waveform of the TENG is consistent with other literature [28,32–34] and includes a positive peak and a negative peak, as shown in Fig. 2d. As shown in Fig. S4: (i) After the water droplets impacted many times, the FEP surface accumulated some negative charges. (ii) After the water droplets impact the FEP, the water droplets diffuse on the FEP surface. When the diffused water droplet touches the TENG top electrode, the positive charge of the TENG bottom electrode is rapidly transferred to the TENG top electrode (the positive peak starts to appear). The positive charge transfer ends when the contact area between the water droplet and the TENG top electrode expands to the maximum (the positive peak ends). (iii) During the droplet retraction stage, the contact area between the droplet and the top electrode of the TENG starts to decrease, and the positive charge starts to flow back (the start of the negative peak) until the droplet leaves the top electrode completely. (iv) When the droplet slides completely off the top electrode, the generation cycle of TENG finishes (negative peak ends). The

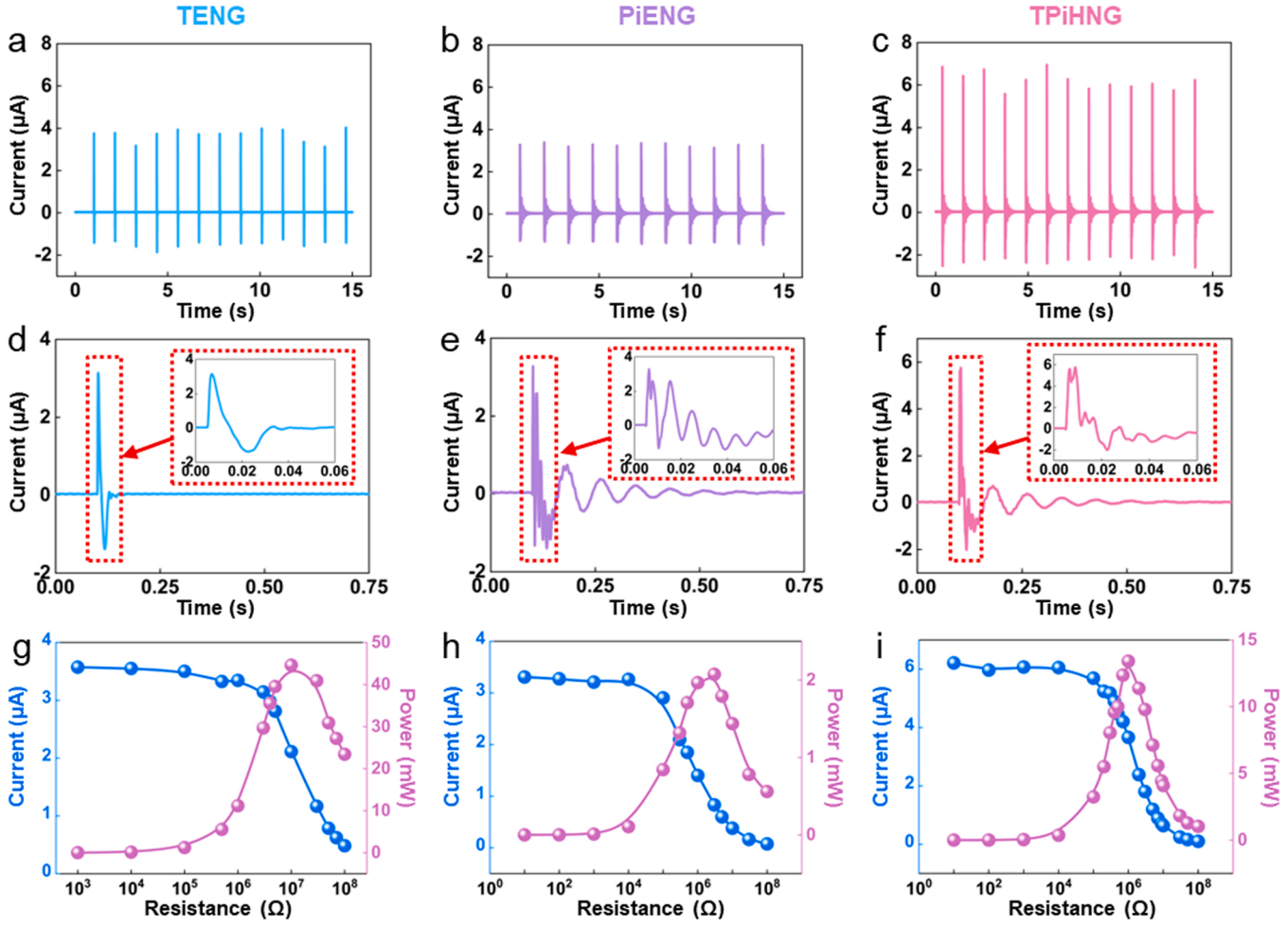

Fig. 2. Electrical performance of TPiHNG. Currents of (**a**) TENG, (**b**) PiENG and (**c**) TPiHNG. Individual current waveforms of (**d**) TENG, (**e**) PiENG and (**f**) TPiHNG. Current power diagrams of (**g**) TENG, (**h**) PiENG and (**i**) TPiHNG.

waveform of PiENG is a bit more complicated than that of TENG, as shown in Fig. 2e. When the droplet touches the FEP, PiENG immediately responds to the droplet impact by deforming along with the cantilever beam. Before the water droplet leaves the cantilever beam, the cantilever beam does forced vibration under the water droplet load, and PiENG also produces the output under forced vibration with the cantilever beam. The vibration frequency of the cantilever beam under forced vibration is the same as the frequency of the water droplet load. After the water droplet leaves the cantilever beam, the cantilever beam does damped free vibration, and PiENG also produces the output under damped free vibration with the cantilever beam. The vibration frequency of the cantilever beam under free damped vibration is the same as the intrinsic frequency of the cantilever beam. The waveform of TPiHNG is jointly influenced by TENG and PiENG, retaining the waveform with damped free vibration in PiENG (Fig. 2f). The voltage measurement result is shown in Fig. S5. The voltage of TENG is 27.6 V. The voltage of PiENG is 1.4 V. Since TENG and PiENG are connected in parallel, the voltage of TPiHNG is only 2.7 V. The current and power of TENG, PiENG and TPiHNG with different resistances were also investigated. The optimal impedance of TENG is 10 MΩ and the maximum power is 44.6 mW (Fig. 2g). As shown in Fig. 2h, the optimal impedance of PiENG is 3 MΩ and the maximum power is 2.1 mW. As shown in Fig. 2i, the optimal impedance of TPiHNG is 1 MΩ and the maximum power is 13.4 mW. Because the TENG and PiENG are connected in parallel, the optimal impedance of the TPiHNG is smaller than that of the TENG and PiENG. The impedance of the TPiHNG is only one-tenth that of the TENG, leading to the maximum power of the TPiHNG being smaller than that of the TENG. With 1 M resistance in series, the electrical energy and energy conversion efficiency of TENG are 0.04708 μJ and 0.0094%, respectively, while those of PiENG are 0.04369 μJ and 0.0084%, respectively. The calculation of electrical energy and energy conversion efficiency is shown in Note. S1.

The current waveform of TPiHNG is obtained by adding the current waveform of PiENG and the current waveform of TENG. Different current waveforms of PiENG and different current waveforms of TENG result in different current waveforms of TPiHNG. PiENG and TENG do not necessarily respond simultaneously. The current waveform of TPiHNG is not only affected by the current waveform of PiENG and the current waveform of TENG, but also by the response time difference between PiENG and TENG. Define the response time difference between PiENG and TENG as the time when TENG starts to respond minus the time when PiENG starts to respond. As shown in Fig. 3a, when PiENG and TENG respond simultaneously, the first two peaks of the TPiHNG current waveform are about the same height. When PiENG responds 1.8 ms earlier than TENG, the current waveform of TPiHNG changes significantly. Compared with the situation when PiENG and TENG respond simultaneously, the first peak of the TPiHNG current waveform becomes lower, the second peak becomes higher, and the TPiHNG maximum current becomes larger. It can be seen that the response time difference between PiENG and TENG has a great influence on the TPiHNG current waveform, therefore it is important to study the response time difference between PiENG and TENG.

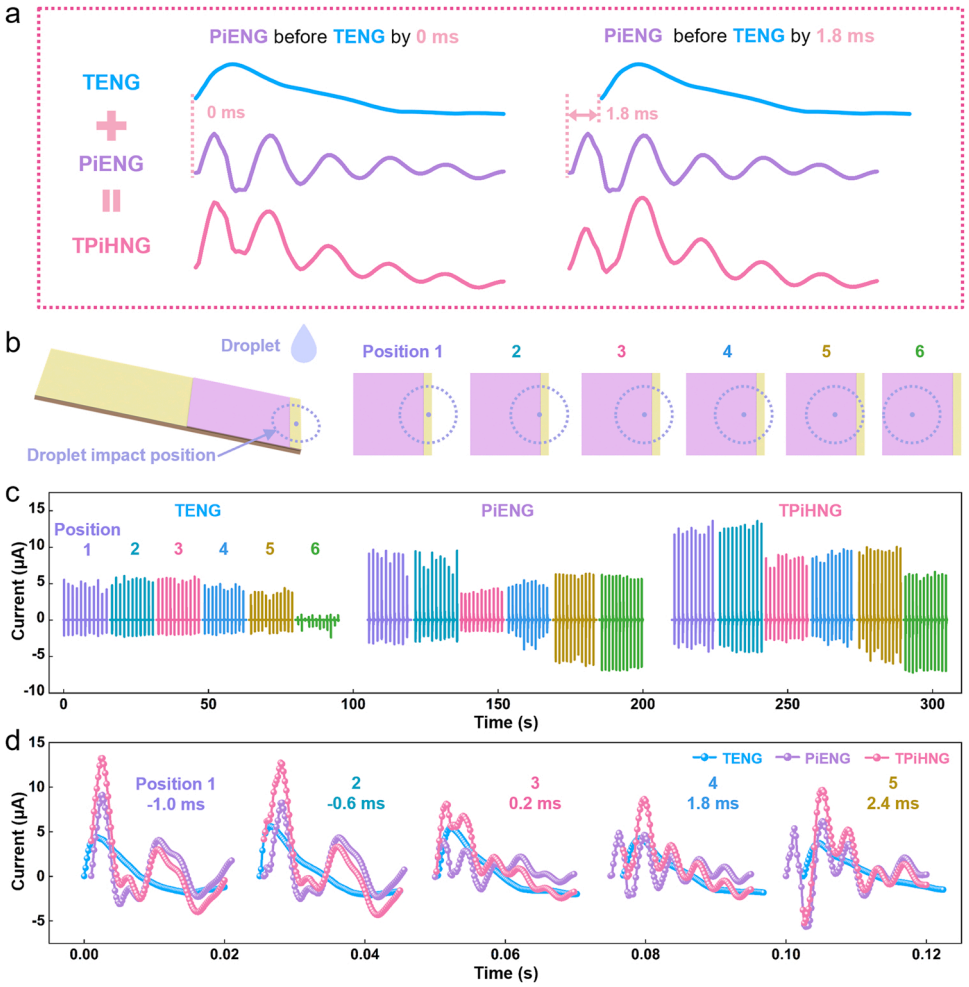

Fig. 3. Effect of response time difference between PiENG and TENG and the effect of water droplet impact position on the electrical performance of TPiHNG. (**a**) Effect of the response time difference between PiENG and TENG on the current waveform of TPiHNG. (**b**) The effect of water droplet impact position on (**c**) the currents of TENG, PiENG, TPiHNG and (**d**) the response time difference between PiENG and TENG.

We looked into how the water droplet's impact position affected the currents in TENG, PiENG, and TPiHNG. As shown in Fig. 3b, six different water droplet impact positions were investigated. The water droplet impact positions are lined up in a line along the longitudinal direction of the cantilever beam. The dashed line indicates the maximum area profile spread out after the water droplet impact. Position 1 is the position closest to the free end of the cantilever beam where the stable TENG signal appears. The distances from position 2 to position 6 away from position 1 are 2 mm, 6 mm, 10 mm, 15 mm and 22 mm, respectively. The water droplet impact positions can be divided into three regions according to the maximum current classification of TENG, PiENG, and TPiHNG. Different regions have different maximum current features. The first region contains position 1 and position 2. There is part of water leaving the cantilever beam when the water droplet spreads to the maximum area, which makes the cantilever beam vibrate faster. Therefore, the maximum current of PiENG is larger, as shown in Fig. 3c. The maximum current of TPiHNG is also larger. The second region contains position 3, position 4 and position 5. There is less water leaving the cantilever beam when the water droplet spreads to the maximum area, which causes the cantilever beam to vibrate a little slower than the first region. Therefore, the maximum current of PiENG is smaller. The maximum current of PiENG increases as the position approaches the fixed end of the cantilever beam. the maximum current of TENG is maximum at the optimal droplet impact position. The maximum current of TENG decreases gradually as the droplet impact position gets farther and farther from the optimal position. The third area contains position 6. The water droplet impact location is far from the top electrode. The water does not touch the top electrode when the water droplet is spread out at the maximum area after impact. This results in negligible maximum current for TENG. The maximum current of TPiHNG in this region is about as large as the maximum current of PiENG.

Since the current of TENG in position 6 is negligible, there is no response time difference between PiENG and TENG in position 6. We investigated the effect of different impact positions from position 1 to position 5 on the response time difference between PiENG and TENG. During the measurement, we have only one Keithley 6514. The currents of TENG, PiENG, and TPiHNG were measured sequentially with the Keithley 6514. The current data of 15 s from TENG, PiENG, and TPiHNG are taken for analysis respectively. Due to the random character of water droplet impact, not all current waveforms are the same even though the experimental conditions are identical. The waveform characteristics are statistically analyzed. The waveform characteristics generally include the time from the initial to the highest peak and the highest peak value. The waveform whose time is the median and the highest peak near the average of the highest peak is selected as the typical waveform from the 15 s data. The typical waveforms of TENG and PiENG are added together according to different relative response times. The relative response time in the added waveform that is most similar to the typical waveform of TPiHNG is taken as the relative response time. Fig. 3d shows the typical waveforms of TENG and PiENG and their added waveforms (equivalent to the typical waveform of TPiHNG). The time interval between the adjacent data points in Fig. 3d is 0.2 ms. As shown in Fig. 3d, from position 1 to position 5, PiENG responds − 1.0 ms, − 0.6 ms, 0.2 ms, 1.8 ms, and 2.4 ms faster than TENG. The water droplet's impact position has a significant effect on the response time difference between PiENG and TENG. PiENG reacts more quickly than TENG as the water droplet's impact position moves further away from the cantilever beam's free end. When the water droplet impacts the cantilever beam, the current of PiENG starts to appear. The TENG current starts to emerge when the water droplet contacts the top electrode. This is the reason why the impact position of water droplet affects the response time difference between PiENG and TENG. Therefore, by adjusting the distance from the impact position to the top electrode when the water droplet falls, the response time difference between PiENG and TENG can be changed.

The slope angle is defined as the angle α formed by the cantilever beam and the horizontal plane. The position of the water droplet impact has a significant impact on the current. It is difficult to assure the consistency of the water droplet impact position when the slope angle is significant. The impacts of various minor slope angles on TENG, PiENG, TPiHNG currents, and the response time difference between PiENG and TENG are investigated. The small slope angles were taken as 10, 20 and 30 degrees, respectively. In the figure, the current is taken as 15 s and the individual current waveform is taken as 0.02 s. We adjusted the height of the droplet relative to the ground when the angle was changed to ensure that the height of the droplet relative to the TENG (droplet falling height) was always constant. Since the droplet falling height is constant, the kinetic energy is constant. So, the kinetic energy has no effect on the maximum current of TENG and PiENG. The increase in slope angle causes the water droplet to slide over the top electrode faster. The reduction in charge transfer time causes the maximum current of TENG to become larger [33]. Therefore, the maximum current of TENG increases with the increase of slope angle as shown in Fig. 4a. The stiffness of the cantilever beam has an effect on the maximum current of the PiENG. When the stiffness is infinite, the cantilever beam will not deform, then PiENG will not generate current. When the stiffness is close to 0, the cantilever beam deforms at the same rate as the droplet falls, and the maximum current of PiENG will be large. As the slope angle is larger, the stiffness of the cantilever beam is smaller. From Fig. 4a, it can be seen that the maximum current of PiENG is almost constant. Therefore, it could be inferred that the change in stiffness due to the slope angle from 10 to 30 degrees has little effect on the maximum current of PiENG. The maximum current of TPiHNG is increased with the increase of angle by TENG. At 10, 20, and 30 degrees, the response time difference between PiENG and TENG is 0.6, 0.6, and 0.8 ms, respectively. It shows that the effect of different small slope angles on the response time difference between PiENG and TENG is quite small.

The effect of different water droplet falling heights on the currents of TENG, PiENG, TPiHNG and the response time difference between PiENG and TENG was investigated. Four different water droplet falling heights were measured, which were 55, 70, 85 and 100 centimeters. As shown in Fig. 4b, the maximum current of the TENG increases from 55 cm to 85 cm for the water droplet falling height. As the releasing height increases, the kinetic energy of the falling water droplets becomes larger. The water droplet has a larger diffusion area on the FEP surface, which results in more charge. Therefore, the maximum current of the TENG increases with the increase of height. The maximum current of TENG for water droplet falling height of 100 cm is slightly lower than that of 85 cm. When the height is too high, the splash of water droplets after impact causes the diffusion area to become smaller. Therefore, there is a decrease in the maximum current [52]. The output current of the previous solid-liquid TENG started to decrease when the release height exceeded 20 cm. In this work the current at a height of 85 cm is a bit larger than that of 20 cm (Fig. S6). Compared with the previous support structure of solid-liquid TENGs, the cantilever beam structure has lower stiffness. The cantilever beam structure has a cushioning effect when the water droplet falls, which can mitigate or avoid the splashing of water droplets. Compared with the previous solid-liquid TENGs, the solid-liquid TENG with cantilever beam structure has a higher releasing height when current decrease occurs. As the water droplet falling height increases, the maximum current of PiENG is increasing. According to the law of conservation of energy, the higher the droplet falling height, the higher the velocity of the droplet when it hits the cantilever beam. The current of piezoelectricity is proportional to the strain rate, so the maximum current of PiENG is proportional to the water droplet falling height. The maximum current of TPiHNG increases with the increase of water droplet falling height due to the effect of PiENG. As shown in Fig. S7, the energy conversion efficiency of PiENG increases slightly with the increase of height. The energy conversion efficiency of TPiHNG also decreases due to the large decrease in the energy conversion efficiency of TENG. The velocity of the water droplet does not always increase with the increase of height. The viscosity resistance of the water

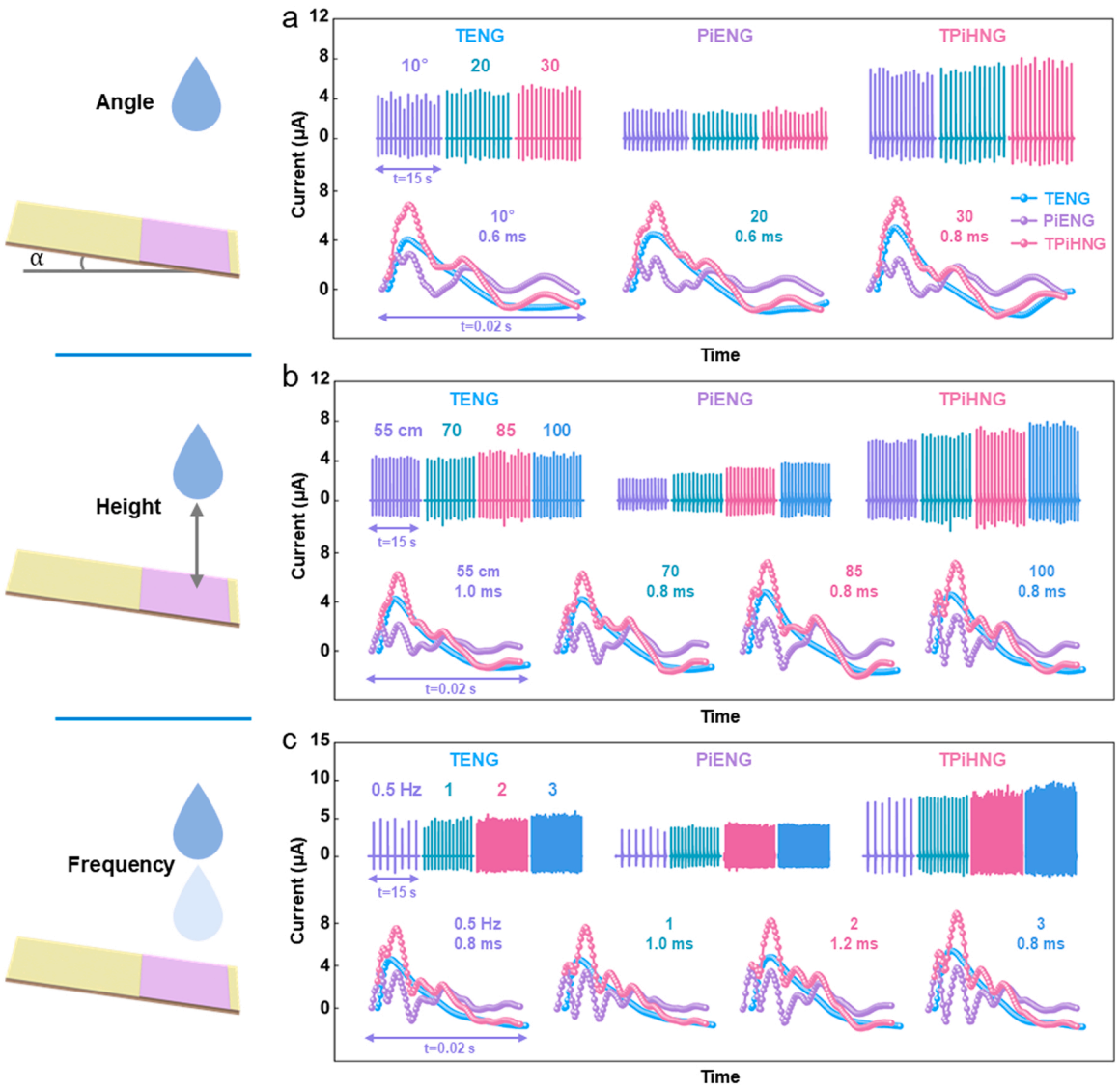

Fig. 4. The effects of the slope angle of the cantilever beam and the water droplet falling parameters on the electrical performance of the TPiHNG. The effects of (**a**) slope angle, (**b**) falling height and (**c**) falling frequency of water droplets on the currents of TENG, PiENG, TPiHNG and the response time difference between PiENG and TENG.

droplet in the air increases with the increase of velocity. When it increases to a certain value, the viscosity resistance is equal to the gravity, and the water droplet will keep a uniform rectilinear motion. Therefore, after reaching a certain height, the energy output of PiENG will not continue to increase. The calculation of energy conversion efficiency (R=10 kΩ) is shown in Note. S1. The response time differences between PiENG and TENG for water droplet falling heights of 55 cm, 70 cm, 85 cm and 100 cm were 1.0 ms, 0.8 ms, 0.8 ms and 0.8 ms, respectively. It indicates that the effect of different water droplet falling heights on the response time difference between PiENG and TENG is quite small.

We investigated the effect of water droplet falling frequency on the currents of TENG, PiENG, TPiHNG and the response time difference between PiENG and TENG. Four different water droplet falling frequencies were measured, which were 0.5 Hz, 1 Hz, 2 Hz and 3 Hz. The charges generated by triboelectrification do not have enough time to escape or be neutralized under the high frequency impact of water droplets. As shown in Fig. 4c, the increase in the transferred charge due to the increase in frequency leads to an increase in the maximum current of the TENG [34]. The output current of TENG is 4.58 μA, 4.62 μA, 4.84 μA and 5.32 μA for 0.5–3 Hz. The output current of TENGs increases proportionally with the frequency. As the water droplet falling frequency gets closer to the resonant frequency (13 Hz) of the cantilever beam, the vibration speed of the cantilever beam is increasing. Therefore, the maximum current of PiENG is increasing as the water droplet falling frequency increases. And the maximum current of TPiHNG increases as the water droplet falling frequency increases. The response time differences between PiENG and TENG for water droplet falling frequencies of 0.5 Hz, 1 Hz, 2 Hz and 3 Hz were 0.8 ms, 1.0 ms, 1.2 ms and 0.8 ms, respectively, indicating that the effect of different water droplet falling frequencies on the response time differences between PiENG and TENG is small.

In addition to the investigation of the water droplet falling parameters and the slope angle, we also investigated the parameters of the water droplet itself. At first, we studied the effect of the water source of the water droplets on the currents of TENG, PiENG, TPiHNG and the response time difference between PiENG and TENG. Ultrapure water, pure water and tap water were selected for the study. As shown in Fig. 5a, the maximum current for ultrapure water is minimal. The maximum current of pure water is greater than the maximum current of tap water. The main difference between ultrapure water, pure water and tap water is the ion concentration. The ion concentration in pure water and tap water is greater than that of ultrapure water. The ions in the

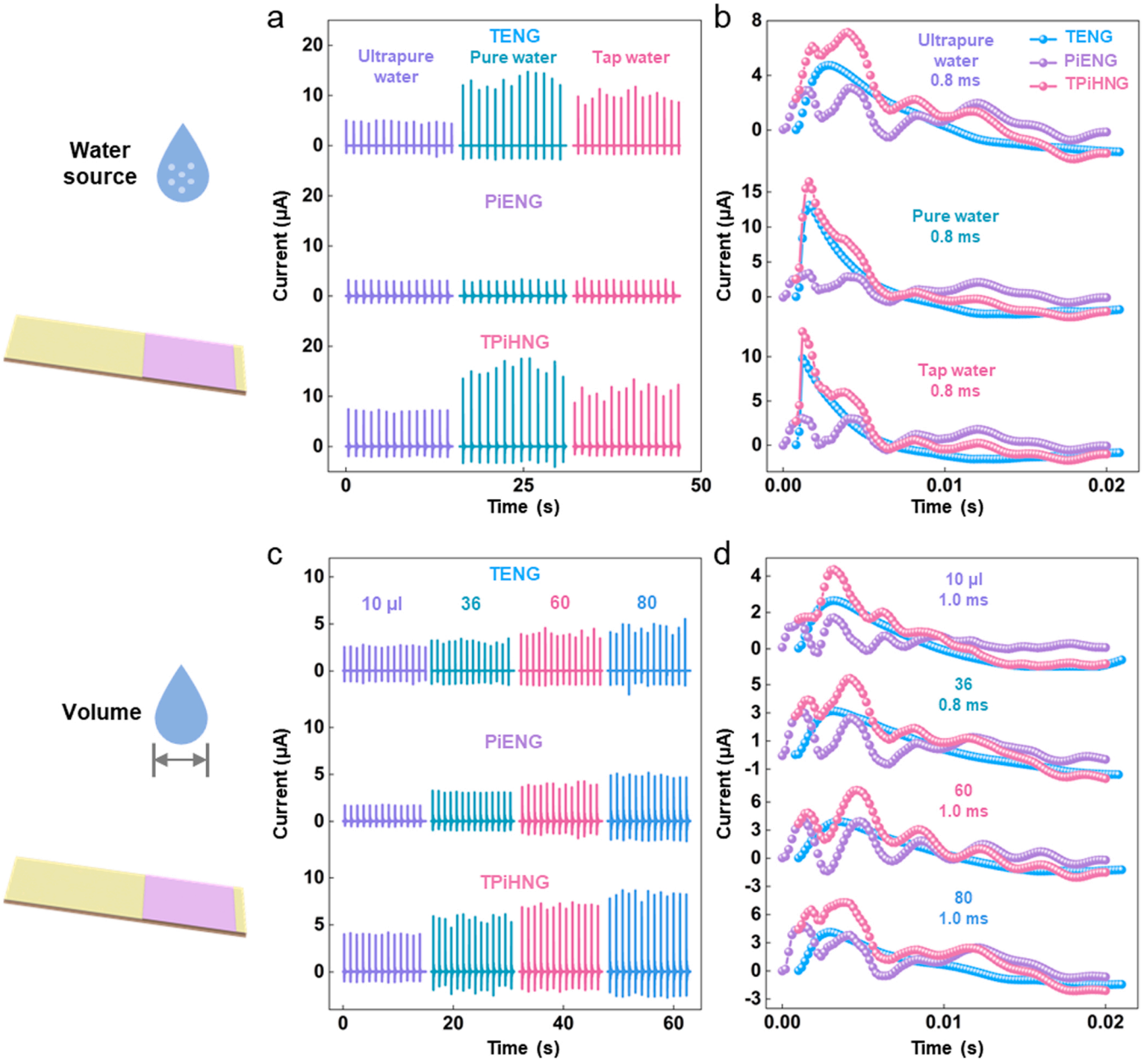

Fig. 5. The effect of the parameters of the water droplet itself on the electrical performance of the TPiHNG. The effect of the water source of the water droplet on (**a**) the currents of TENG, PiENG, TPiHNG and (**b**) the response time difference between PiENG and TENG. The effect of the volume of the water droplet on (**c**) the currents of TENG, PiENG, TPiHNG and (**d**) the response time difference between PiENG and TENG.

aqueous solution can reduce the resistance of the aqueous solution to improve the output performance. When the ion concentration exceeds the appropriate concentration, the leakage of capacitors and the screening effect from the triboelectric layer will occur, resulting in a reduction in current [53]. Since the water source of water droplets has almost no effect on the kinetic energy, the water source of water droplets has almost no effect on the maximum current of PiENG. The maximum current of TPiHNG of pure water is the largest due to the influence of TENG. As shown in Fig. 5b, the current waveform of TENG is not the same for different water sources. Pure water and tap water reach the current peak of TENG faster than ultrapure water. The response time difference between PiENG and TENG for ultrapure water, pure water and tap water are all 0.8 ms. It shows that the effect of different water source on the response time difference between PiENG and TENG is very small. Then we also investigated the effect of the water droplet volume on the currents of TENG, PiENG, TPiHNG and the response time difference between PiENG and TENG. The chosen water droplet volumes were 10 μl, 36 μl, 60 μl and 80 μl. Due to the increase in the volume of the water droplet, the kinetic energy becomes larger. Therefore, the maximum current of PiENG is increasing. The increase of water droplet volume brings more charge. Therefore, the maximum current of TENG is increasing as the volume of water droplet increases. Since the maximum current of PiENG and TENG increases, the maximum current of TPiHNG also increases. As shown in Fig. 5d, the response time differences between PiENG and TENG for 10 μl, 36 μl, 60 μl and 80 μl were 1.0 ms, 0.8 ms, 1.0 ms and 1.0 ms, respectively. It indicates that the effects of different water droplet volumes on the response time differences between PiENG and TENG were small.

4. Conclusion

In conclusion, we propose a new design strategy to increase the

current of the water droplet nanogenerator through combining TENG and PiENG to simultaneous scavenge of the mechanical energy of the liquid-solid contact of the water droplets and the deformation energy of the substrate. Under the strategy, the TPiHNG with cantilever beam structure is designed to increase the piezoelectric current. Compared with the bottom fixed structure, the piezoelectric current of the cantilever beam structure increases from 0.2 μA to 3.3 μA. The TPiHNG has a significantly higher current (3.7 μA) compared to TENG (6.2 μA). The response time difference between PiENG and TENG is proposed for the first time as an important parameter of TPiHNG. The response time difference is controlled by changing the water droplet falling position. The effects of impact position, slope angle, falling height, falling frequency, water source and volume on the currents of TENG, PiENG, TPiHNG and the response time difference between PiENG and TENG were investigated. This work provides a novel approach to scavenge water droplet energy more efficiently.

Future work focuses on device integration and parameter optimization. The performance of hybrid generators can be improved by parameter optimization of TENG and PiENG. For TENG, the output performance can be improved by selecting friction materials, adjusting dielectric layer thickness and adjusting external load [51]. For PiENG, it can be designed with piezoelectric materials with larger piezoelectric coefficients and lower stiffness support structures to improve the output performance. The performance of hybrid nanogenerators can be improved by integrating the devices into planar arrays [54].

CRediT authorship contribution statement

Y.H., Y.Y. and Y.S. supervised the research and conceived the idea. M.Z., C.B. and C.H. carried out the device fabrication and the performance measurement. M.Z., Y.H., Y.Y. and Y.S. analyzed the data and co-wrote the manuscript. All authors read and revised the manuscript.

Declaration of Competing Interest

The authors declare that they have no known competing financial interests or personal relationships that could have appeared to influence the work reported in this paper.

Data availability

No data was used for the research described in the article.

Acknowledgments

This work was supported by the National Natural Science Foundation of China (Grant No. 12172359), Beijing Municipal Natural Science Foundation (Grant No. 2202066), Key Research Program of Frontier Sciences of the Chinese Academy of Sciences (Grant No. ZDBS-LY-JSC014), CAS Interdisciplinary Innovation Team (Grant No. JCTD-2020–03), the National Key R&D Project from the Minister of Science and Technology in China (Grant No. 2021YFA1201604), the National Natural Science Foundation of China (Grant No. 52072041), the Beijing Natural Science Foundation (Grant No. JQ21007), the University of Chinese Academy of Sciences (Grant No. Y8540XX2D2), Opening fund of State Key Laboratory of Nonlinear Mechanics (Grant No. LNM202207), State Key Laboratory of Digital Manufacturing Equipment and Technology, Huazhong University of Science and Technology (Grant No. DMETKF2022014).

Appendix A. Supporting information

Supplementary data associated with this article can be found in the online version at doi:10.1016/j.nanoen.2022.107992.

References

[1] S. Chu, A. Majumdar, Opportunities and challenges for a sustainable energy future, Nature 488 (2012) 294–303.
[2] O. Ellabban, H. Abu-Rub, F. Blaabjerg, Renewable energy resources: current status, future prospects and their enabling technology, Renew. Sustain. Energy Rev. 39 (2014) 748–764.
[3] V. Sebestyen, Renewable and sustainable energy reviews: environmental impact networks of renewable energy power plants, Renew. Sustain. Energy Rev. 151 (2021).
[4] T. Tsoutsos, N. Frantzeskaki, V. Gekas, Environmental impacts from the solar energy technologies, Energy Policy 33 (2005) 289–296.
[5] S. Jeong, M.D. McGehee, Y. Cui, All-back-contact ultra-thin silicon nanocone solar cells with 13.7% power conversion efficiency, Nat. Commun. 4 (2013).
[6] Z.Y. Fan, A. Javey, PHOTOVOLTAICS Solar cells on curtains, Nat. Mater. 7 (2008) 835–836.
[7] S.H. Wang, X. Wang, Z.L. Wang, Y. Yang, Efficient scavenging of solar and wind energies in a smart city, ACS Nano 10 (2016) 5696–5700.
[8] S.M. Lu, A global review of enhanced geothermal system (EGS), Renew. Sustain. Energy Rev. 81 (2018) 2902–2921.
[9] S.-Y. Pan, M. Gao, K.J. Shah, J. Zheng, S.-L. Pei, P.-C. Chiang, Establishment of enhanced geothermal energy utilization plans: Barriers and strategies, Renew. Energy 132 (2019) 19–32.
[10] I.B. Fridleifsson, Geothermal energy for the benefit of the people, Renew. Sustain. Energy Rev. 5 (2001) 299–312.
[11] D. Egré, J.C. Milewski, The diversity of hydropower projects, Energy Policy 30 (2002) 1225–1230.
[12] C. Zarfl, A.E. Lumsdon, J. Berlekamp, L. Tydecks, K. Tockner, A global boom in hydropower dam construction, Aquat. Sci. 77 (2015) 161–170.
[13] S.H. Wang, X.J. Mu, Y. Yang, C.L. Sun, A.Y. Gu, Z.L. Wang, Flow-driven triboelectric generator for directly powering a wireless sensor node, Adv. Mater. 27 (2015) 240–248.
[14] A. Ahmed, I. Hassan, M. Hedaya, T. Abo El-Yazid, J. Zu, Z.L. Wang, Farms of triboelectric nanogenerators for harvesting wind energy: A potential approach towards green energy, Nano Energy 36 (2017) 21–29.
[15] B. Chen, Y. Yang, Z.L. Wang, Scavenging wind energy by triboelectric nanogenerators, Adv. Energy Mater. 8 (2018).
[16] W.X. Zhu, C.S. Hu, C.R. Bowen, Z.L. Wang, Y. Yang, Scavenging low-speed breeze wind energy using a triboelectric nanogenerator installed inside a square variable diameter channel, Nano Energy 100 (2022).
[17] S. Roga, S. Bardhan, Y. Kumar, S.K. Dubey, Recent technology and challenges of wind energy generation: A review, Sustain. Energy Technol. Assess. 52 (2022).
[18] N. Gupta, A review on the inclusion of wind generation in power system studies, Renew. Sustain. Energy Rev. 59 (2016) 530–543.
[19] P.L. Fan, M.S. Cho, Z.H. Lin, Z.T. Ouyang, J.G. Qi, J.Q. Chen, E.F. Moran, Recently constructed hydropower dams were associated with reduced economic production, population, and greenness in nearby areas, Proc. Natl. Acad. Sci. U. S. A. 119 (2022).
[20] J.S. Hecht, G. Lacombe, M.E. Arias, T.D. Dang, T. Piman, Hydropower dams of the Mekong River basin: a review of their hydrological impacts, J. Hydrol. 568 (2019) 285–300.
[21] F.R. Fan, Z.Q. Tian, Z.L. Wang, Flexible triboelectric generator!, Nano Energy 1 (2012) 328–334.
[22] X. Wang, Y. Yang, Effective energy storage from a hybridized electromagnetic-triboelectric nanogenerator, Nano Energy 32 (2017) 36–41.
[23] L.X. Gao, X. Chen, S. Lu, H. Zhou, W.B. Xie, J.F. Chen, M.K. Qi, H. Yu, X.J. Mu, Z. L. Wang, Y. Yang, Enhancing the output performance of triboelectric nanogenerator via grating-electrode-enabled surface plasmon excitation, Adv. Energy Mater. 9 (2019).
[24] H. Ryu, H.M. Park, M.K. Kim, B. Kim, H.S. Myoung, T.Y. Kim, H.J. Yoon, S.S. Kwak, J. Kim, T.H. Hwang, E.K. Choi, S.W. Kim, Self-rechargeable cardiac pacemaker system with triboelectric nanogenerators, Nat. Commun. 12 (2021).
[25] H.M. Wang, L. Xu, Y. Bai, Z.L. Wang, Pumping up the charge density of a triboelectric nanogenerator by charge-shuttling, Nat. Commun. 11 (2020).
[26] W.L. Liu, Z. Wang, G. Wang, G.L. Liu, J. Chen, X.J. Pu, Y. Xi, X. Wang, H.Y. Guo, C. G. Hu, Z.L. Wang, Integrated charge excitation triboelectric nanogenerator, Nat. Commun. 10 (2019).
[27] L. Zheng, Z.H. Lin, G. Cheng, W.Z. Wu, X.N. Wen, S.M. Lee, Z.L. Wang, Silicon-based hybrid cell for harvesting solar energy and raindrop electrostatic energy, Nano Energy 9 (2014) 291–300.
[28] W.H. Xu, H.X. Zheng, Y. Liu, X.F. Zhou, C. Zhang, Y.X. Song, X. Deng, M. Leung, Z. B. Yang, R.X. Xu, Z.L. Wang, X.C. Zeng, Z.K. Wang, A droplet-based electricity generator with high instantaneous power density, Nature 578 (2020) 392.
[29] S.-B. Jeon, D. Kim, G.-W. Yoon, J.-B. Yoon, Y.-K. Choi, Self-cleaning hybrid energy harvester to generate power from raindrop and sunlight, Nano Energy 12 (2015) 636–645.
[30] F. Zhan, A.C. Wang, L. Xu, S. Lin, J. Shao, X. Chen, Z.L. Wang, Electron transfer as a liquid droplet contacting a polymer surface, ACS Nano 14 (2020) 17565–17573.
[31] H. Cho, J. Chung, G. Shin, J.-Y. Sim, D.S. Kim, S. Lee, W. Hwang, Toward sustainable output generation of liquid–solid contact triboelectric nanogenerators: The role of hierarchical structures, Nano Energy 56 (2019) 56–64.
[32] W. Xu, Z. Wang, Fusion of slippery interfaces and transistor-inspired architecture for water kinetic energy harvesting, Joule 4 (2020) 2527–2531.
[33] N. Tang, Y. Zheng, M. Yuan, K. Jin, H. Haick, High-performance polyimide-based water–solid triboelectric nanogenerator for hydropower harvesting, ACS Appl. Mater. Interfaces 13 (2021) 32106–32114.

[34] N. Zhang, H. Gu, K. Lu, S. Ye, W. Xu, H. Zheng, Y. Song, C. Liu, J. Jiao, Z. Wang, X. Zhou, A universal single electrode droplet-based electricity generator (SE-DEG) for water kinetic energy harvesting, Nano Energy 82 (2021), 105735.
[35] W. Xu, X. Li, J. Brugger, X. Liu, Study of the enhanced electricity output of a sliding droplet-based triboelectric nanogenerator for droplet sensor design, Nano Energy 98 (2022), 107166.
[36] J.H. Lee, S. Kim, T.Y. Kim, U. Khan, S.-W. Kim, Water droplet-driven triboelectric nanogenerator with superhydrophobic surfaces, Nano Energy 58 (2019) 579–584.
[37] J. Peng, L. Zhang, W. Sun, Y. Liu, D. Yang, M. Feng, Y. Feng, D. Wang, High-efficiency droplet triboelectric nanogenerators based on arc-surface and organic coating material for self-powered anti-corrosion, Appl. Mater. Today (2022), 101564.
[38] L. Zhao, L. Liu, X. Yang, H. Hong, Q. Yang, J. Wang, Q. Tang, Cumulative charging behavior of water droplet driven freestanding triboelectric nanogenerators toward hydrodynamic energy harvesting, J. Mater. Chem. A 8 (2020) 7880–7888.
[39] Y. Yang, C. Lee, Making use of water droplets as a sustainable green energy source, Droplet 1 (2022) 7–10.
[40] Z.L. Wang, J.H. Song, Piezoelectric nanogenerators based on zinc oxide nanowire arrays, Science 312 (2006) 242–246.
[41] H.L. Zhou, Y. Zhang, Y. Qiu, H.P. Wu, W.Y. Qin, Y.B. Liao, Q.M. Yu, H.Y. Cheng, Stretchable piezoelectric energy harvesters and self-powered sensors for wearable and implantable devices, Biosens. Bioelectron. 168 (2020).
[42] Z.B. Yang, S.X. Zhou, J. Zu, D. Inman, High-performance piezoelectric energy harvesters and their applications, Joule 2 (2018) 642–697.
[43] S.H. Wang, Z.L. Wang, Y. Yang, A. One-Structure-Based, Hybridized nanogenerator for scavenging mechanical and thermal energies by triboelectric-piezoelectric-pyroelectric effects, Adv. Mater. 28 (2016) 2881–2887.
[44] Y. Ji, K.W. Zhang, Y. Yang, A. One-Structure-Based, Multieffects coupled nanogenerator for simultaneously scavenging thermal, solar, and mechanical energies, Adv. Sci. 5 (2018).
[45] X.T. Xu, Y.L. Wang, P.Y. Li, W.H. Xu, L. Wei, Z.K. Wang, Z.B. Yang, A leaf-mimic rain energy harvester by liquid-solid contact electrification and piezoelectricity, Nano Energy 90 (2021).
[46] Y.W. Su, S. Li, Y. Huan, R. Li, Z.H. Zhang, P. Joe, C. Dagdeviren, The universal and easy-to-use standard of voltage measurement for quantifying the performance of piezoelectric devices, Extrem. Mech. Lett. 15 (2017) 10–16.
[47] H.C. Liu, J.W. Zhong, C. Lee, S.W. Lee, L.W. Lin, A comprehensive review on piezoelectric energy harvesting technology: Materials, mechanisms, and applications, Appl. Phys. Rev. 5 (2018).
[48] J.W. Zhou, L.P. He, L. Liu, G. Yu, X.F. Gu, G.M. Cheng, Design and research of hybrid piezoelectric-electromagnetic energy harvester based on magnetic couple suction-repulsion motion and centrifugal action, Energy Convers. Manag. 258 (2022).
[49] Z.Y. Zhou, W.Y. Qin, P. Zhu, S.J. Shang, Scavenging wind energy by a Y-shaped bi-stable energy harvester with curved wings, Energy 153 (2018) 400–412.
[50] J. Briscoe, N. Jalali, P. Woolliams, M. Stewart, P.M. Weaver, M. Cainb, S. Dunn, Measurement techniques for piezoelectric nanogenerators, Energy Environ. Sci. 6 (2013) 3035–3045.
[51] N. Zhang, H. Zhang, W. Xu, H. Gu, S. Ye, H. Zheng, Y. Song, Z. Wang, X. Zhou, A droplet-based electricity generator with ultrahigh instantaneous output and short charging time, Droplet 1 (2022) 56–64.
[52] X. Chen, C.H. Jiang, Y.H. Song, B.B. Shao, Y.F. Wu, Z.H. Song, T. Song, Y.S. Wang, B.Q. Sun, Integrating hydrovoltaic device with triboelectric nanogenerator to achieve simultaneous energy harvesting from water droplet and vapor, Nano Energy 100 (2022), 107495.
[53] L. Xie, L. Yin, Y. Liu, H. Liu, B. Lu, C. Zhao, T.A. Khattab, Z. Wen, X. Sun, Interface engineering for efficient raindrop solar cell, ACS Nano 16 (2022) 5292–5302.
[54] Y. Song, W. Xu, Y. Liu, H. Zheng, M. Cui, Y. Zhou, B. Zhang, X. Yan, L. Wang, P. Li, X. Xu, Z. Yang, Z. Wang, Achieving ultra-stable and superior electricity generation by integrating transistor-like design with lubricant armor, Innovation 3 (2022), 100301-100301.

Maoyi Zhang is now pursuing his Ph.D. degree in Institute of Mechanics, Chinese Academy of Sciences, China. He received her bachelor's degree in Engineering Mechanics from Dalian University of Technology in 2017. His current research interests include flexible sensors and energy harvesters.

Chengmin Bao is studying for a doctor's degree at Minzu University of China. She is currently a visiting student in the research group of Professor Ya Yang at Beijing Institute of Nanoenergy and Nanosystems, Chinese Academy of Sciences (CAS). She obtained her bachelor's and master's degree in environmental science from Tianjin University in 2009 and 2012 respectively. Her current research interest is triboelectric nanogenerator.

Chaosheng Hu is currently a doctoral candidate in the research group of Prof. Ya Yang at Beijing Institute of Nanoenergy and Nanosystems, Chinese Academy of Sciences (CAS). His research interests are focused on triboelectric nanogenerator and ferroelectric material.

Prof. YongAn Huang received his B.S. degree (2001), M.S. degree (2004), and Ph.D. degree (2007) from the Northwestern Polytechnical University, Xian, China. He is the vice director of the State Key Laboratory of Digital Manufacturing Equipment and Technology (SKL-DMET), Huazhong University of Science and Technology (HUST). He was awarded the Outstanding Young Scholar of NSFC. His research interests include flexible electronics manufacturing and advanced printing.

Prof. Ya Yang received his Ph.D. in Materials Science and Engineering from University of Science and Technology Beijing, China. He is currently a professor at Beijing Institute of Nanoenergy and Nanosystems, Chinese Academy of Sciences, China. His main research interests focus on ferroelectric materials and devices for energy conver-sion, self-powered sensing, and some new physical effects. He has published one book and more than 200 SCI academic papers in Science Advances and other journals. These papers have been cited by more than 17000 times, and the corresponding H-index is 80. He is the Editor-in-Chief of Nanoenergy Advances and is the editorial committee member of InfoMat, Nano-Micro Letters, Nanoscale, iScience, Nanoscale Advances, and some other journals. He is the Guest Editor of Research, iScience, Nanomaterials, and Energies. Details can be found at: http://www.researcherid.com/rid/A-7219–2016.

Prof. Yewang Su received his Ph.D. from Tsinghua University, Beijing, China. He is currently a professor at Institute of Mechanics, Chinese Academy of Sciences, China. His research focuses on flexible and stretchable sensors in the field of sensing the curvature, large strain, and pressure et al. He is now finding the new application of flexible and stretchable sensors on wearable devices and the intelligent industry. He has been published more than 80 SCI papers in peer reviewed high-level scientific journals and held more than 20 patents in his research area.